Technical Design of a Shrouded Small-Scale Turbine

Prepared for: Collegiate Wind Competition

Prepared by: **Wildcat Wind Power**
Lawryn Edmonds, President - EE
Lee Evans, Vice President - ME
Caitlin Ingham, Treasurer
Jake Meyer, Secretary - EE
ME Team Lead, Alex Dzewaltowski
EE Team Lead, Broden Bowell
Dr. Ruth Douglas Miller, Adviser
Dr. Warren White, Adviser
Additional EE Team Members - 8
Additional ME Team Members - 6

KANSAS STATE
College of Engineering

Table of Contents

List of Figures

List of Tables

List of Abbreviations

Executive Summary

Wildcat Wind Power (WWP) is an extracurricular, engineering, design team. Our mission is to design, build, and test a small-scale wind turbine to compete in the Collegiate Wind Competition (CWC). This year's CWC will include testing turbines with winds of varying directions as a new aspect to consider in our design. The main design goals our of team this year included yaw capabilities, maximizing the coefficient of power, and minimizing the cut-in speed of our wind turbine. To meet these goals, the turbine we designed this year is a horizontal-axis, 5-blade turbine equipped with a shroud.

In our efforts to achieve these goals, we have designed our turbine to include a shroud while retaining the passive pitch hub from last year's competition turbine. The shroud is a diverging diffuser located directly behind the rotor. Its purpose is to create a low-pressure region behind the turbine rotor which increases the wind speed incident on the rotor. Multiple academic articles were our inspiration for a shrouded design. Furthermore, our own testing verifies that a shrouded turbine increases performance over a comparably-sized, unshrouded wind turbine. The way the shroud connects the nacelle to the tower provides passive yaw so the wind turbine can adapt to changes in wind direction. The rotor hub incorporates a mechanical system that passively controls the pitch of the blades. This is not for speed regulation but is done to maintain higher performance characteristics over a wider range of wind speeds.

Unique techniques were implemented electrically to optimize the performance of our wind turbine. Primarily, the rectified voltage output from the generator is either bucked down or boosted up. This is done through our custom-made DC-DC converter in order to safely supply constant power to our microcontroller, an Arduino Uno. Additionally, a maximum-power-point tracker (MPPT) was implemented in our design to optimize the power output through manipulation of the duty cycle of the buck-boost converter. With this control, we can increase or decrease the speed of the generator to achieve the maximum power point through an iterative process based on the previous power calculation. Our microcontroller also controls braking for safety and regulation of our turbine. The braking system relies on back electromagnetic force (EMF) of the generator when the three phases are tied to ground through use of a relay shield on an Arduino. Braking occurs when the microcontroller detects a manual button press, a loss of load, or the wind speed is greater than 11 m/s. The microcontroller receives input from a current sensor. With measured current and a known voltage level, the load will display a power and energy value.

Wildcat Wind Power conducted turbine tests with our wind tunnel that was designed and constructed by team members specifically for participation in the CWC. Our wind tunnel was modified for this year's competition so that we could test our turbine's yaw capabilities. Utilizing these resources to refine and optimize a design, WWP will present an efficient and innovative turbine at competition.

1.0 Introduction

This conceptual design report represents Kansas State University's design submission for the Department of Energy's 2017 Collegiate Wind Competition. Our design is a horizontal axis wind turbine (HAWT) with electrical components to achieve and maintain a minimum 10W continuous output at wind speeds above 11 m/s. This report covers the mechanical and electrical design elements of the turbine, and the testing thereof. The mechanical analysis outlines the design and test results of the blades, hub, shroud, and yaw control for the turbine. The electrical analysis consists of an overview of the generator, rectifier, brake, DC-DC converter, maximum power point tracker, load, and microcontroller.

2.0 Mechanical Design

The major mechanical components of our HAWT include a shroud, nacelle, tower, hub, and blades. The design includes a shroud as a way to decrease cut-in speed, increase our coefficient of power, and provide torque for yaw control. The nacelle was designed to support the shroud as well as house the electrical components. The tower has been designed to accommodate yawing while supporting the turbine assembly. A passive, variable-pitch hub and blade assembly was selected to increase efficiency in changing wind speeds. The final design is shown in Figure 21 of the appendix.

2.1 Shroud

This year, we started investigating shroud designs and found some promising results from Flannery, Holligan, and Soares [1]. They found that their design increased velocity by a factor of 1.47 and energy yield increased by a factor of 3.18. Another shrouded wind turbine system by Ohyn and Karasudani in the Journal Energies, outlines a brimmed diffuser with improved performance over standard HAWTs [2]. Their design showed a promising increase of 2-5 times more power produced compared to a standard HAWT with a given wind swept area and wind speed.

A shroud increases the mass flow rate of air through the opening by creating a low-pressure zone behind the shroud. Due to size restriction, it was important for us to develop the optimal shroud design that would both increase mass flow and best utilize the given area. Using SolidWorks FloXpress analysis we modeled several designs to determine which had the highest flow increase [3]. This included shrouds with circular inlet/outlets as well as one that featured a circular inlet with a square outlet. These designs were modeled with and without a flange around the outside of the outlet. From this analysis, we found that the optimum design was a shroud that is circular at both the inlet and outlet and has a square flange at the outlet, as shown in Figure 1, on the next page. This shroud increased wind speed by 45% and improved performance by 12% over the next best shroud design.
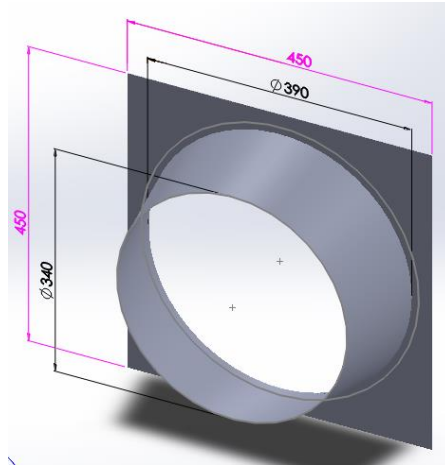
Figure 1. Initial shroud design; units in millimeters.

After the modifications to our tunnel were completed this fall, we began testing our own prototype to verify the improvements for ourselves. Due to the unique shape, 3-D printing would have been ideal for constructing this design. However, the volume of printed material required to produce a sturdy product was not cost effective for a prototype. Instead, two sheets of 0.06" thick ABS plastic were used. A 2-D arch was measured, cut out and glued into a ring to produce the 3-D conical diffuser. This was then secured to a square cut sheet of plastic acting as the flange. Shortened blades were 3-D printed in order to fit in the shroud inlet. This shroud was attached to the existing turbine, used in last year's competition, and tested in the wind tunnel shown in Figure 2. Data were collected with the shortened blades and the shroud and with the full-length blades without the shroud.

Figure 2. Test configuration of shroud prototype.

We confirmed that the turbine with the shroud displayed a significant increase in performance over the turbine without the shroud with our test data, shown in Figure 20 on page 17. We then began working on a final design to be 3-D printed. We wanted to improve the turbine's stability while incorporating a passive yaw system. This meant we needed to transmit electrical power through the tower using a slip ring. Some changes were not incorporated into the first prototype due to time constraints, while other more intricate design features could only be implemented with 3-D printing technology.

The first feature we modified was the diffuser profile. According to compact diffuser tests performed by Ohya and Karasudani, C-profile diffusers produced a higher power coefficient than similar straight-profile designs [2]. Changing our Solidworks model profile from straight to C-shaped was a quick and straightforward modification, and one that could only be implemented using a 3-D printer. These changes are presented in Figure 3, below. Both inlet and outlet diameters were kept the same as the prototype's. To more easily allow for airstream intake on the outer fringe of the inlet, a curved nozzle was also added. This provided the shroud with additional rigidity. Additional material was added to the bottom of the shroud for support and to allow for easy connection to the tower.
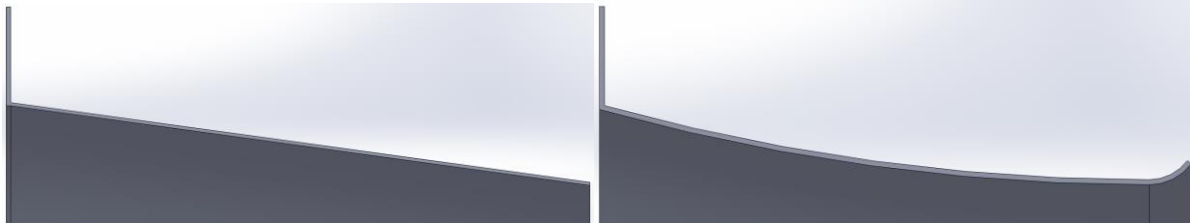
Figure 3. Straight shroud profile (left) and C-shaped shroud profile (right).

Since our shroud with a brim is 17.7" (45 cm) wide, it was unable to fit in the 16" x 14" printer. To work around this, the team divided the shroud into three pieces. At the seams, we modeled in an overlapping lip to add rigidity and provide a surface with which we could easily glue the sections together. Due to the fact that 3-D printing was not required to make the back square flange, it was removed from the 3-D printed model. Instead, a similar flanged lip was modeled and constructed on the back edge to which a larger ABS square flange could be glued. Our final shroud design, without the square flange, is shown in Figure 4. The hole in the bottom of the shroud allows for the passage of the electrical wiring. Figures 21 and 22 of the appendix show dimensioned drawings of our final shroud design.
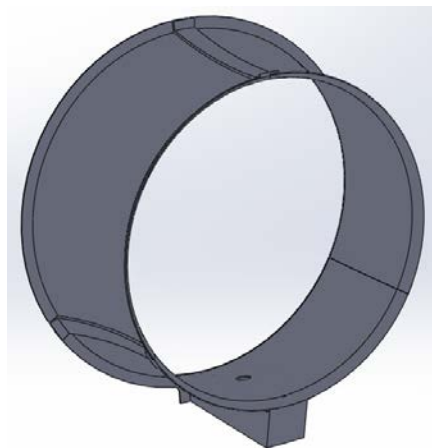
Figure 4. Final shroud design.

Our next challenge was to modify our shroud to be yaw-compatible. This involved considering where the tower would be placed, and how it would be fixed to the shroud in a way that would provide stability. When it came to tower location, the team decided to place the tower as close to the front of the shroud as possible. This would allow the majority of the surface area of the shroud to act as a wind vane.

The comparison of small-scale wind turbines by Cui, Yu, Liu, and Whitty, allowed us to intuitively design a shrouded wind turbine that will align with the incident wind [4]. Incident wind can impact the rotor

4

cross section at an angle, where the component normal to the rotor cross section is the force on the rotor. The thrust on the rotor is represented as

$$F_t = \frac{1}{2}C_t\rho(V\cos\delta)^2 S_t$$

where C_t is the thrust parameter, ρ is the density of air, and S_t is the wind swept area of the rotor. The side-force is expressed as

$$F_s = \frac{1}{2}C_s\rho(V\sin\delta)^2 A_s$$

where C_s is the side-force coefficient, and A_s is the projected side area. The resulting moment created by the thrust on the turbine is given by

$$M_t = F_t d = \frac{1}{2}C_t\rho(V\cos\delta)^2 S_t d$$

where d is the distance of the yaw axis from the rotor axis. Similarly, the moment caused by the side-force is given as

$$M_s = F_s l = \frac{1}{2}C_s\rho(V\sin\delta)^2 A_s l$$

where l is the distance between the yaw axis and rotor plane. The wind forces can be seen in Figure 5 from a top view.
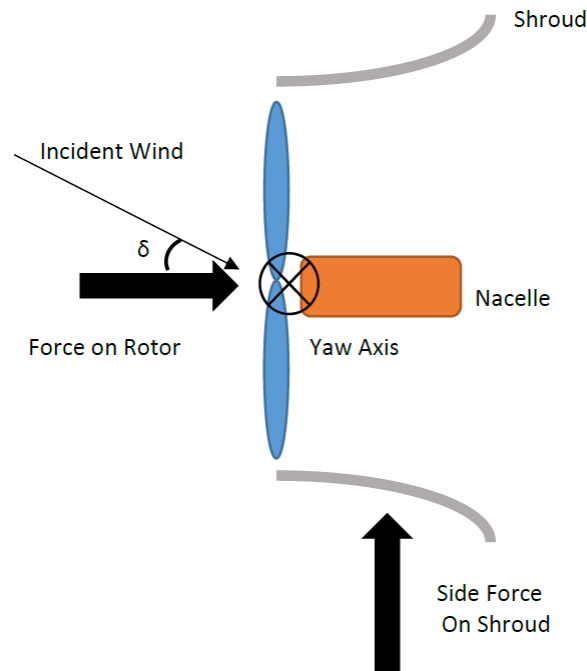
Figure 5. Induced forces from wind on the shroud design.

These induced moments about the yaw axis will eventually settle to equilibrium. From our wind tunnel and real world experiments, we have seen the equilibrium settle to where the wind vector is normal to rotor plane. We have found adding a brim to the back side of our shroud not only aligns the rotor plane normal to the wind vector better than without a brim, but creates a larger pressure drop from the inlet to the outlet of the shroud. The position of the yaw axis allows the restoring side force on the shroud to

have a greater effect than the force on the rotor. This is due to the moment arm from the side force being four times greater than the moment arm from the force on the rotor.

2.2 Nacelle

We needed to develop a separate structure to support the nacelle and facilitate our plans to connect the tower at the front of the shroud directly below the blades. To accomplish this, we decided to make a cylindrical nacelle with three airfoil-shaped radial posts that connected to each of the shroud segments. Figure 23 in the appendix shows a dimensioned drawing of the nacelle. The posts help to stabilize the shroud while their shape minimizes airflow interference. Each post is hollow, allowing the electrical wiring to run down from the nacelle to the tower. The two posts located on the top of the nacelle were made smaller to allow room for a removable slide cover which gives easy access to the electrical components inside the nacelle. Figure 6 shows the model used for our final nacelle design.
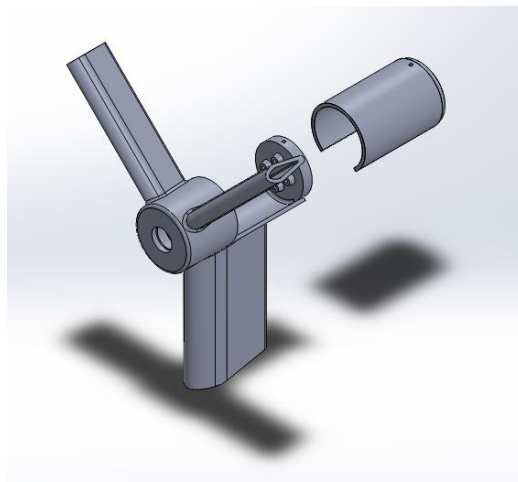
Figure 6. Final nacelle design.

2.3 Tower

An aluminum tube was used as the main component of the tower. This tube was attached to the shroud using two low-friction bearings which would allow the shroud and nacelle to yaw along with the previously mentioned moments about the yaw axis. The aluminum tube is sufficiently structurally supportive to withstand the nacelle, rotor, and shroud weights many times over. The 1" tube allowed us to fit a three-phase slip ring in the middle of tube shown in Figure 7. We wanted to include a slip ring in order to avoid any problems associated with multiple rotations in a given direction that would stress the wires.

Figure 7. Three phase slip ring inside the tube.

To keep the tower from bending due to high wind speeds, we clamped the tube to the base plate. We wanted a tight fit when inserting the tube into the base plate. This was done by milling out a 1" hole in the center of the base plate and fastening a 1" tube clamp to the plate. The aluminum tower could then be held securely by both the plate and clamp.

We performed a fatigue stress analysis to ensure that the pipe we are using could withstand the moment generated by the wind acting on the shroud. To find the maximum bending moment, we must first estimate the total drag force generated by the shroud and blades. Drag force can be estimated by assuming the shroud is a solid cube. F_D, which is drag force, is given by

$$F_D = \frac{1}{2} C_d \rho A_s V^2$$

where C_d is the drag coefficient, ρ is the density of air, A_s is the projected area, and V is the wind speed. The fatigue stress is

$$\sigma_{max} = \frac{Mc}{I}$$

where σ_{max} is the maximum stress due to bending, M is the bending moment, c is the distance to the bending axis, and I is the area moment of inertia. The corrected endurance limit is

$$S_f = C_{load} C_{size} C_{surf} C_{temp} C_{reliab} S_{f'}$$

where S_f is the corrected endurance limit, C_{load} is the load factor, C_{size} is the size factor, C_{surf} is the surface factor, C_{temp} is the temperature factor, C_{reliab} is the reliability factor, and $S_{f'}$ is the endurance limit. The fatigue factor of safety is given by

$$N_f = \frac{S_f S_{ut}}{\sigma'_a S_{ut} + \sigma'_m S_f}$$

where N_f is the fatigue safety factor, S_{ut} is the ultimate tensile strength, σ'_a is the alternating component of stress, and σ'_m is the mean component of stress. Using these equations, we found a maximum stress of 24.822 MPa and a factor of safety of 6.5. Due to conservative estimates for the

applied force resulting in a high factor of safety, we can confidently say that our tower will be sufficient for supporting the rest of the turbine.

2.4 Hub

To help increase efficiency at varying wind speed, we implemented a passive, variable pitch hub. Passive blade pitch is used to decrease our turbine's cut-in speed while maintaining the high-end revolution per minute (RPM) necessary to achieve maximum power output. By passively adjusting the pitch of the blades, we are able to maintain a maximum torque over a variety of rotor speeds while using no additional power. The design uses centripetal force to guide the blades out along grooves in the hub, causing the pitch angle to change. A spring is used to keep the blades at the maximum pitch angle at lower wind speeds. Figure 8 shows our hub at varying pitch angles.
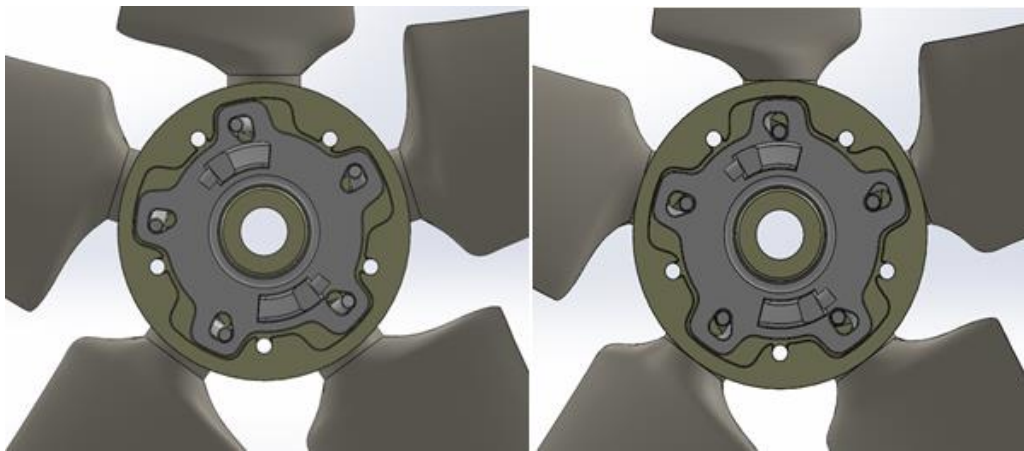
Figure 8. Variable pitch hub.

2.5 Blades

We have designed our blades using the NREL s835 family of airfoils: the s835 for the root section, the s833 for the primary section and the s834 for the tip section. This family of airfoils was specifically designed for variable pitch, horizontal axis wind turbines with rotor diameters of 1-3 meters [5]. The intended 1-3 m rotor diameter of these airfoils is the smallest for which we were able to find data, and should scale well to the size constraints for this project. The chord length of each section was optimized for a tip speed ratio (TSR) of three, providing a wider blade which produces higher torque at low speeds. The airfoil data points were imported into Solidworks along with twist and chord length data from Qblade [6]. This information was used to model the blades which were then 3-D printed. A dimensioned drawing of our blades is shown in Figure 24 of the appendix. The Cp-Lambda plot from our airfoil is shown in Figure 9.
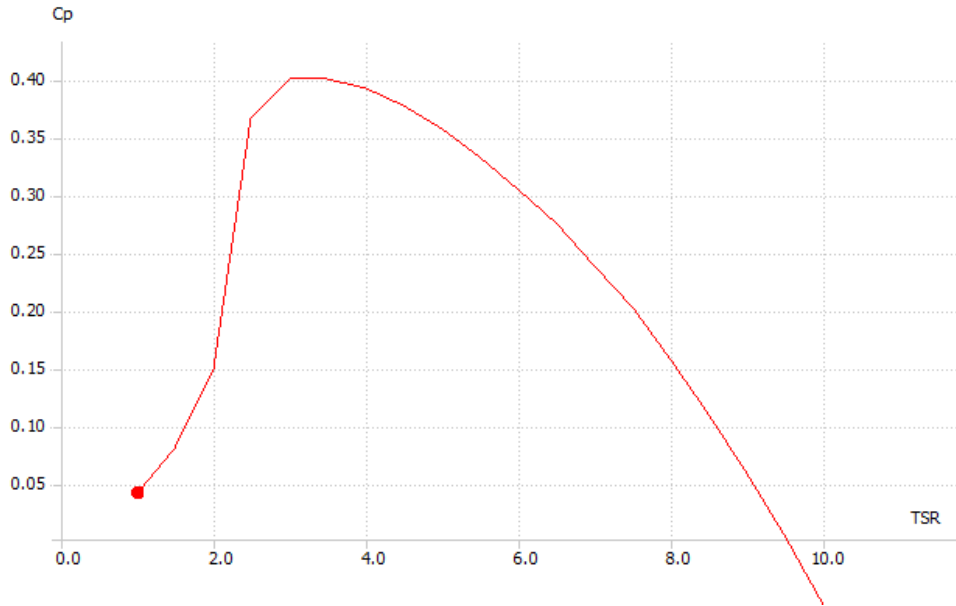
Figure 9. Cp-Lambda plot generated in Q-Blade.

This allowed us to use $\lambda = \frac{4\pi}{n}$, with n = number of blades. The Qblade plot shown in Figure 9 gives a maximum Cp at a TSR of three. Based on this, we can justify our selection of five blades.

Since we incorporated the shroud, we were less concerned with tip losses caused by the vortex effect on the tip of each blade. This induced drag, associated with normal bare wind turbines, can limit the RPM of the rotor. Vortex-induced drag effects are dependent on the ambient air pressure, temperature, and angle of attack. Our shroud acts like an end cap, so the air going around the tip generates less drag than a bare tip would.

After selecting our airfoil, we began testing our prototype shroud and blades to determine the RPM at certain wind velocities. Then, by taking the RPM data, we determined the TSR from the equation below. The results are displayed in Table 1.

$$\lambda = \frac{\text{Tip Speed of Blade}}{\text{Wind Speed}}$$

Table 1. Values for blade RPM and Tip Speed ratio at common wind speeds.

RPM	Tip Speed Ratio
322	1.6
589	2.33
818	2.69
1004	2.83
1200	2.95
1445	3.16
1664	3.27
1882	3.36
2116	3.46

3.0 Electrical Design

The design for the electrical system includes the following six main components: generator, brake, rectifier, DC-DC converter and MPPT, load, and microcontroller. From the generator, the rectifier converts the generated AC voltage into DC for use by the circuit and the load. The microcontroller monitors and automates several of the turbine's processes. These include the brake, current sensor, and voltage measurement. The brake operates by tying the three phases of the generator together, utilizing the back EMF of the generator to decrease the rotational speed of the shaft. Throughout the entire process, the microcontroller takes the input from the current sensor and the voltage measurement to calculate power. A buck-boost DC-DC converter in combination with a maximum-power-point tracker can then be used to affect the speed of the generator and regulate the apparent load impedance to optimize power output. Finally, the load displays performance of the turbine by showing output values and provides a 5V reference.

3.1 Electrical Diagram

Figure 10 and Figure 11 show diagrams detailing the makeup of our circuit. Figure 10 is a simplified block diagram of the power flow through the circuit as well as the general placement of each component relative to the others. Figure 11 is the circuit schematic made using PSpice that shows how all the components are connected. The schematic also shows more specific components such as the two relays for the brake and protection diode. A larger version of Figure 11 is located in the appendix.
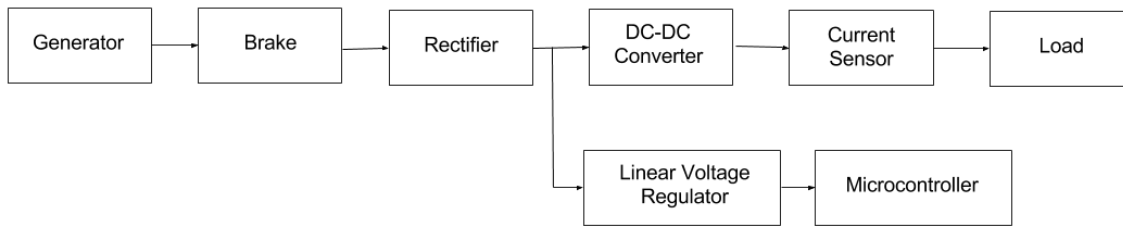
Figure 10. Block diagram showing power flow.
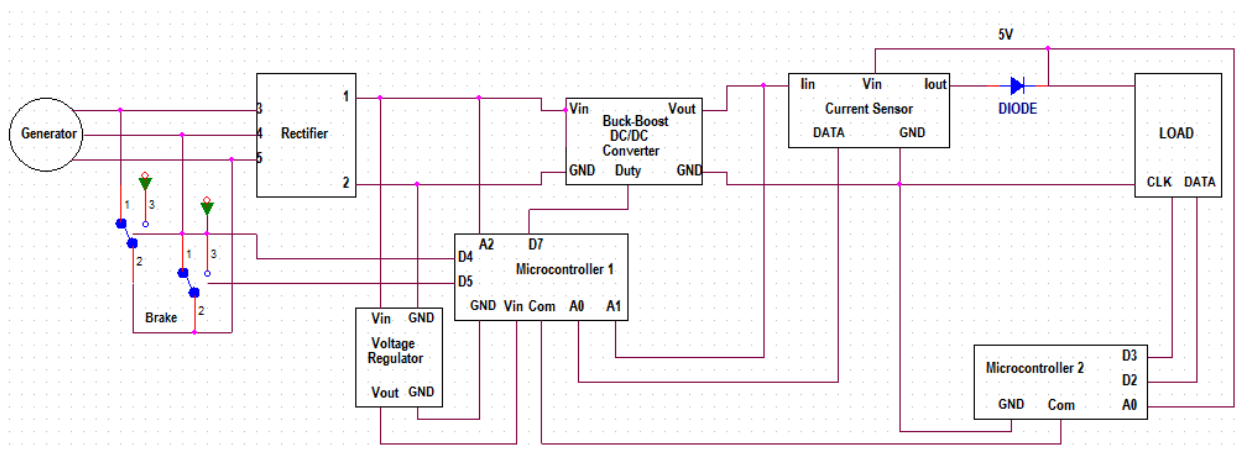
Figure 11. Electrical circuit schematic.

3.2 Generator

Our team tested several generators to find the optimal generator for our application. Of the available generators tested, the team chose to use the LDPower MT4014 330 KV shown in Figure 12 below.

Figure 12. Generator selected for the turbine.

As detailed in the graph in Figure 13, the MT4014 320KV provides the highest excitation voltage of all available generators and relatively low phase to phase resistance. Considering these factors led us to select this generator for our wind turbine.
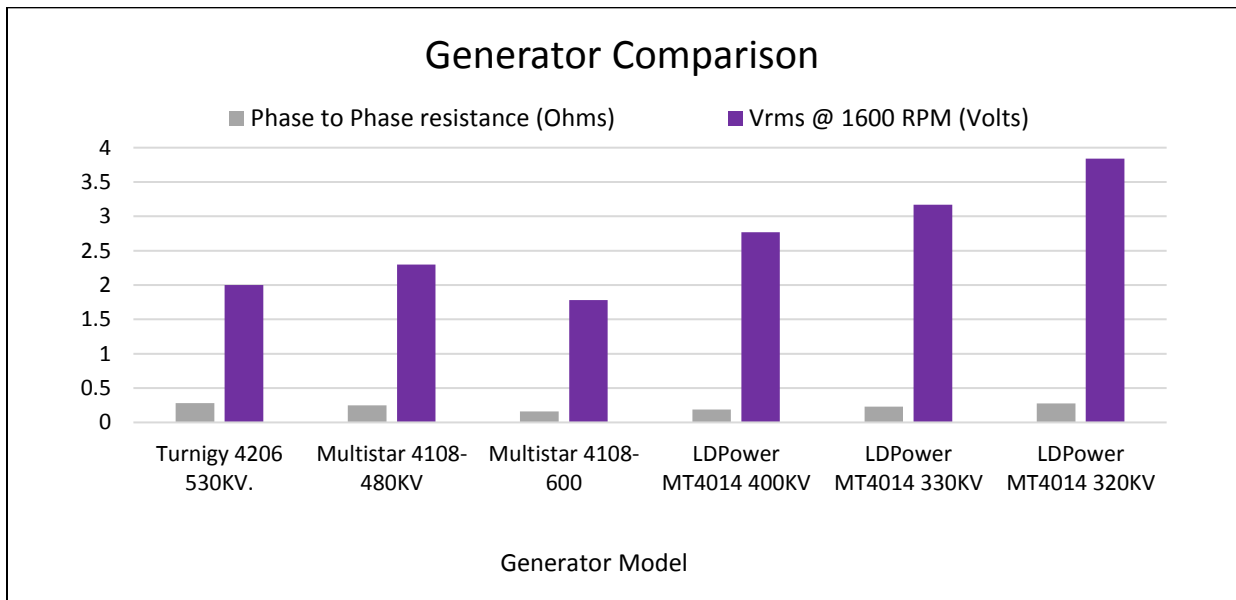
Figure 13. Generator comparison.

The kV rating of a generator relates to the number of stator windings and the gage of wire used to wind the stator. As the kV rating increases, the generator has less stator windings. However, the wires are thicker gage. We chose to go with a 320kV generator which is on the lower end of the kV values we tested. This lower kV allows the motor to generate higher voltages at a lower RPM, which is important

for applications where it is connected to heavy fan blades. Higher voltage ratings require higher RPM to excite the same voltage, making it undesirable for this application.

3.3 Rectifier

The three-phase rectifier is located after the brake. We chose an IXYS FUS-45-0045B three-phase Schottky bridge rectifier. This rectifier provides us with low power losses and a steady DC output with the help of an appropriately sized capacitor. The rectifier has a low voltage drop: approximately 0.55V. This is ideal for our low-voltage, low-power circuit because it reduces the cut-in wind speed. Furthermore, the Schottky three-phase rectifier allows fast switching speeds and low coupling capacity between pins.

3.4 Brake

Our braking system involves taking advantage of the back EMF in the generator. Decreasing the rotational speed of the shaft occurs when the three phases from the generator are tied together. The brake consists of two normally closed (NC) relays being used as switches controlled by the microcontroller. There are two situations in which the brake is activated. When the microcontroller detects a manual button press, power is lost, allowing the relays to close. The other situation simulates a loss of load. This occurs when the point of common coupling is disconnected. When this happens, the turbine control circuit loses power, and the NC relay returns to its normal state, thus decreasing the speed generator. We tested implementing the brake before and after the rectifier. If we were able to place it after the rectifier then we could rectify the system in the nacelle. Rectifying in the nacelle would reduce the number of wires running down the tower from three to two, therefore reducing the magnitude of I^2R losses. However, the brake doesn't significantly reduce the RPM of the generator when placed after the rectifier. While losses increase when the brake is before the rectifier, the brake only meets our team's expectations when placed before the rectifier.

3.5 DC-DC Converter and Maximum Power Point Tracker

We chose to implement a buck-boost DC-DC converter to regulate the voltage at five volts and control the speed of the generator. The topology of this converter is displayed in Figure 14.
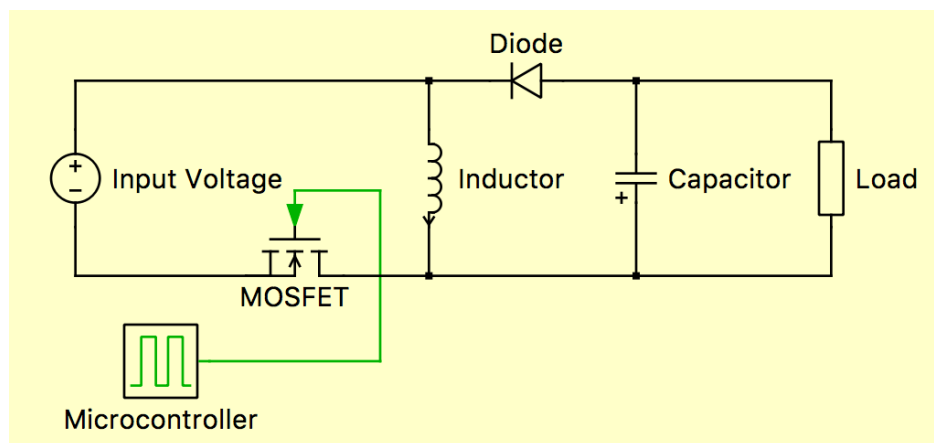
Figure 14. DC-DC converter schematic.

This topology was chosen due to its simplicity. Other more complex topologies for buck-boost converters would allow us to give and/or receive reactive power, which was unnecessary for our current application of the converter. The voltage will be boosted at low RPMs and bucked down at higher RPMs to maintain a consistent voltage output. Our team has chosen to construct a converter instead of buying one off the shelf due to the limited input voltage range of commercial buck-boost converters. However, most of the problems have come from the design and construction of the converter in relation to its hardware side. We discovered that the converter has issues boosting when the impedance of the discrete components is not optimized with the optimal impedance being zero. Test in simulation with an ideal converter are displayed below in Figure 15.
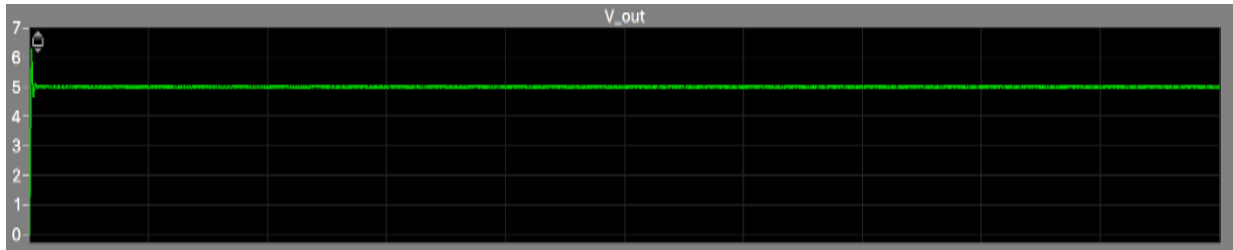
Figure 15. Plot of Output Voltage in simulation of ideal converter over time. (1V/0.1s)

This has led to countless tests of discrete components in attempt to minimize impedances throughout the circuit. However, eliminating impedance entirely from components such as the inductor is impossible. To compensate for this issue, we operate the converter to regulate at six volts, which is lowered to five volts once the losses are accounted for. This operation of the converter is done via maximum power point tracker algorithms to maximize the power output of the generator at all wind speeds. By manipulating the duty cycle of the MOSFET in the converter, we can control the apparent load seen by the generator, which will either increase or decrease the RPM of the generator. This relationship can be seen in the equation below.

$$R_{eq} = R_{load}(1 - D)^2$$

We can see that as duty cycle increases the equivalent resistance seen by the generator will decrease. As the resistance seen by the generator increases, the RPM of the generator will decrease. By utilizing an iterative search, the optimal duty cycle can be found and implemented by reacting to a comparison between current power and the prior iteration's power. This manipulation of the duty cycle creates a feedback loop which can be seen as part of the control state diagram in Figure 17.

3.6 Simulated Load

A physical load shows the power and energy produced by our prototype turbine. The power is shown visually on a small LED display. Our simulated load is a 10 x 12 grid of Neopixel LED lights housed in a frame and shown behind frosted glass. The lights will show pixelated images, such as our club logo. Additionally, it will show two bars that display the power generated at that moment and the total energy produced. The bars will rise up either side as they receive data measured by the current and voltage sensors. Figure 16, below, shows a mock-up design of our competition load. In addition to the LED display, there is a 5V supply acting as a mock battery. This element allows the DC-DC converter to control its input voltage and affect the generator.
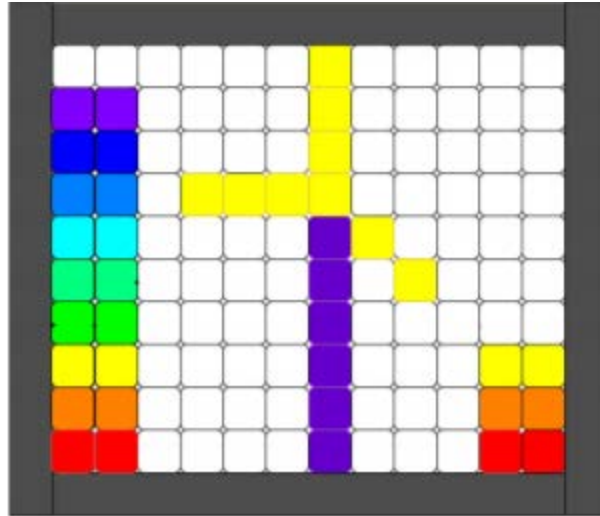
Figure 16. Conceptual load display.

3.7 Microcontroller

The microcontroller monitors and automates several of the circuit's processes. An Arduino Uno was selected for both the turbine and the load display controls. The turbine Arduino receives input signals from the current and voltage sensors. From the current sensor and voltage sensor the turbine Arduino calculates power. If the power is above its rated value, the turbine Arduino will pulse the brake on and off to regulate power output after 11 m/s. If the turbine Arduino detects a manual button press, the brake is initiated. The turbine Arduino sends the voltage and current information to the load Arduino in order to control our display. The control state diagram for this process is depicted in Figure 17.
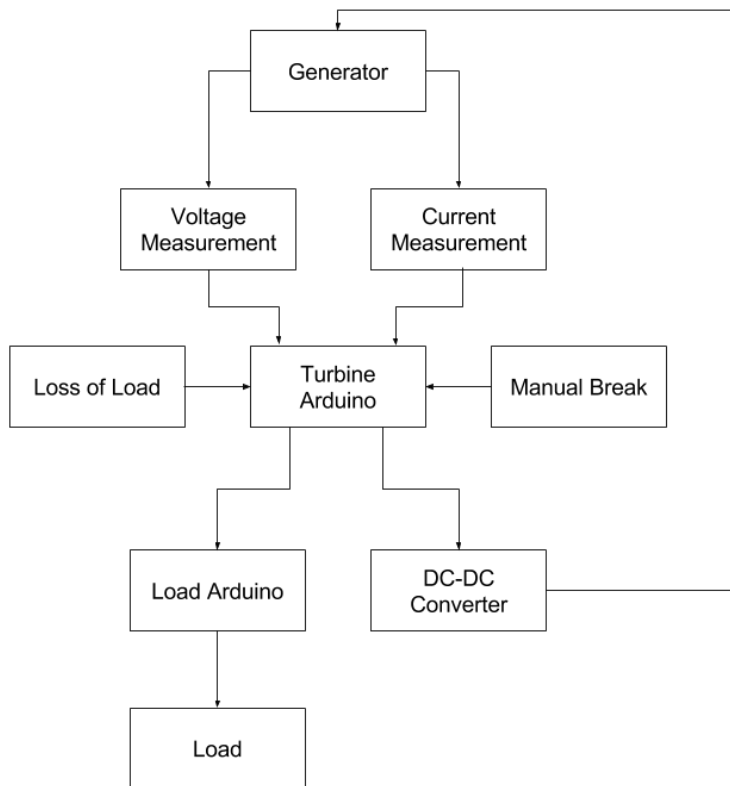
Figure 17. Control state diagram of the electrical circuit.

4.0 Testing Results

Wind tunnel testing on the turbine implementing the shroud showed great promise in increasing our power output. The LabView virtual instrument (VI) and circuit shown in Figures 18 and 19 are what our team used to log our test data when evaluating different generators and when testing our turbine [7].
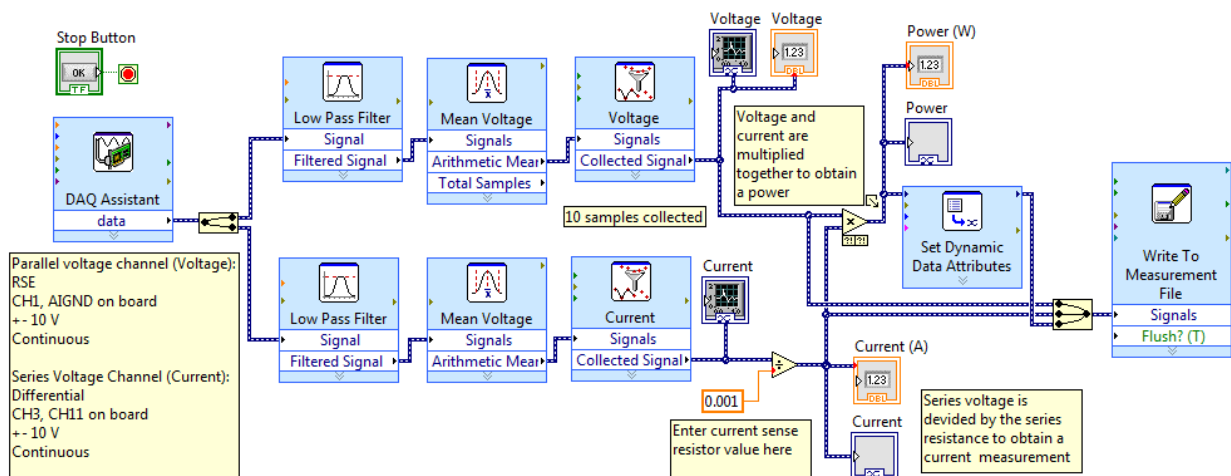
Figure 18. Labview VI used for generator evaluation and turbine testing.
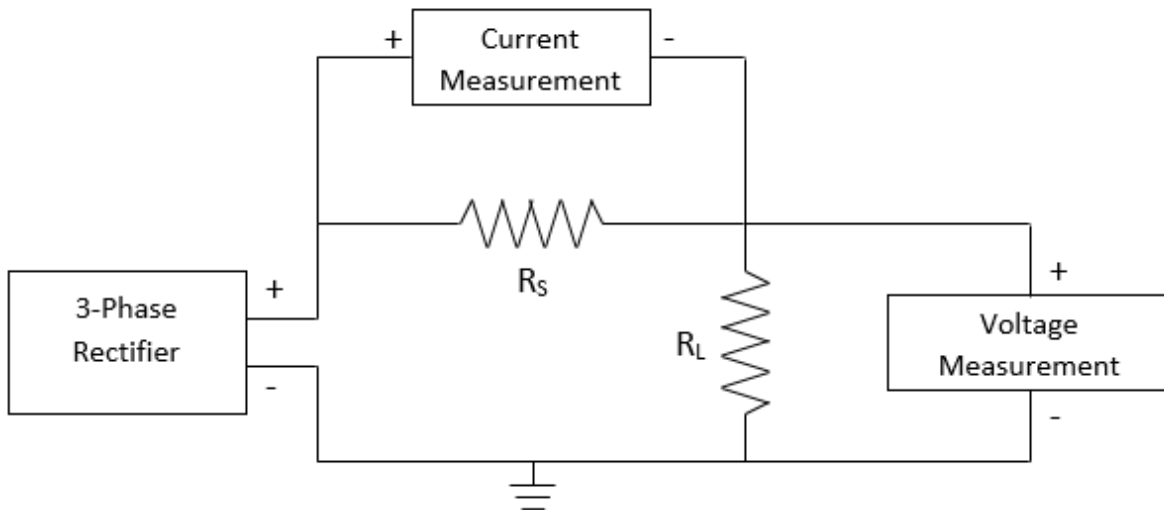
Figure 19. Schematic of power testing setup.

In Figure 19, R_s is a 1 mΩ current sense resistor, and R_L is a 3 Ω load resistor used as a stand-in for our actual load. Therefore, voltage could be measured across the small resistor to calculate the current through our system without supplying a large voltage drop. The voltage measurement was then made across a load resistor. Power was calculated as current multiplied by voltage. This circuit was chosen to imitate the measurement circuit used at competition as best as possible. Data were recorded as wind speed was gradually increased to approximately 10 m/s. The results are shown in Figure 20, below; power is shown as a percent of the maximum measured. The trend displayed in this figure verifies our preliminary research results regarding shrouds with brimmed diffusers.
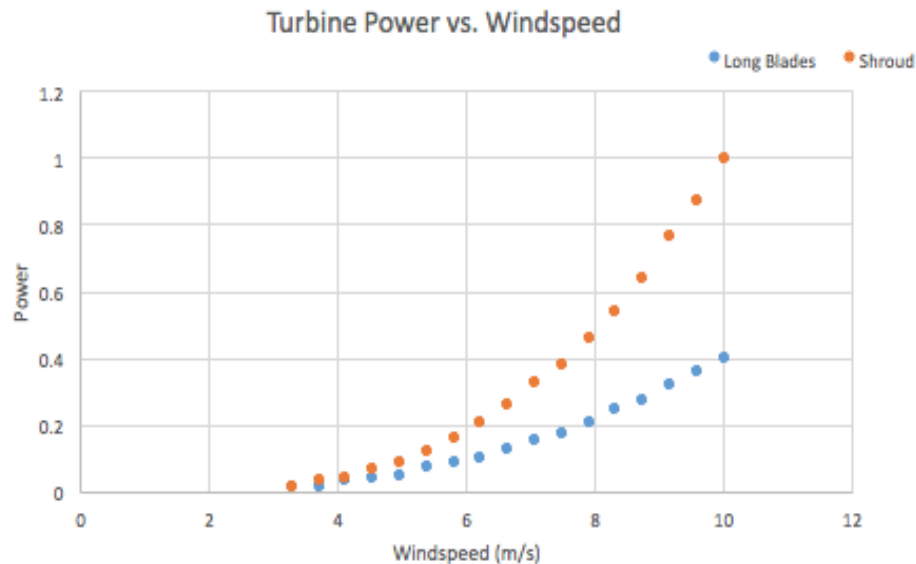
Figure 20. Wind speed data with and without a shroud.

Appendix
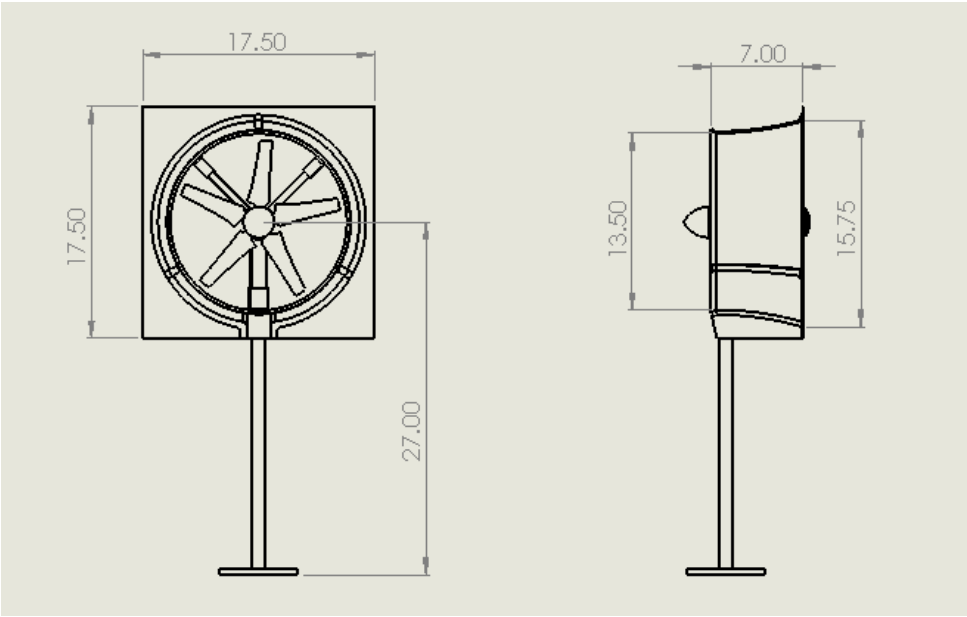
Figure 21. Turbine assembly drawing; units in inches.
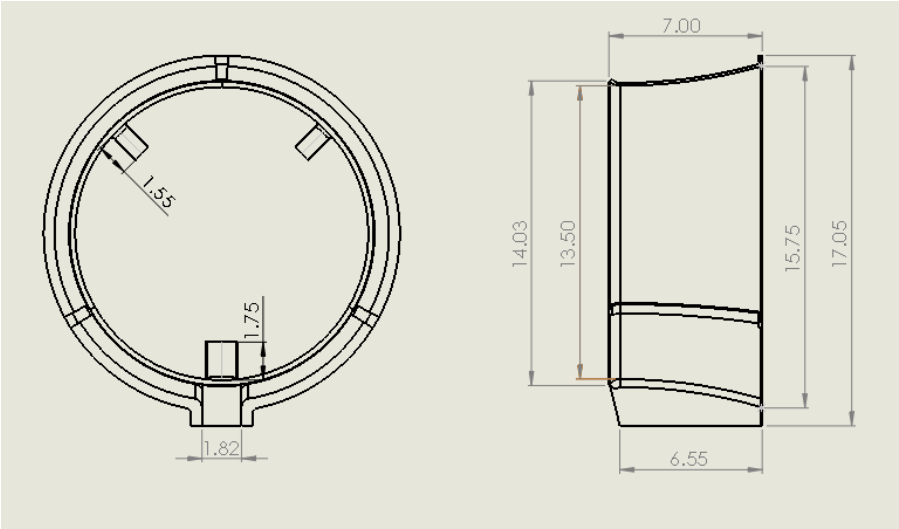
Figure 22. Shroud drawing; units in inches.
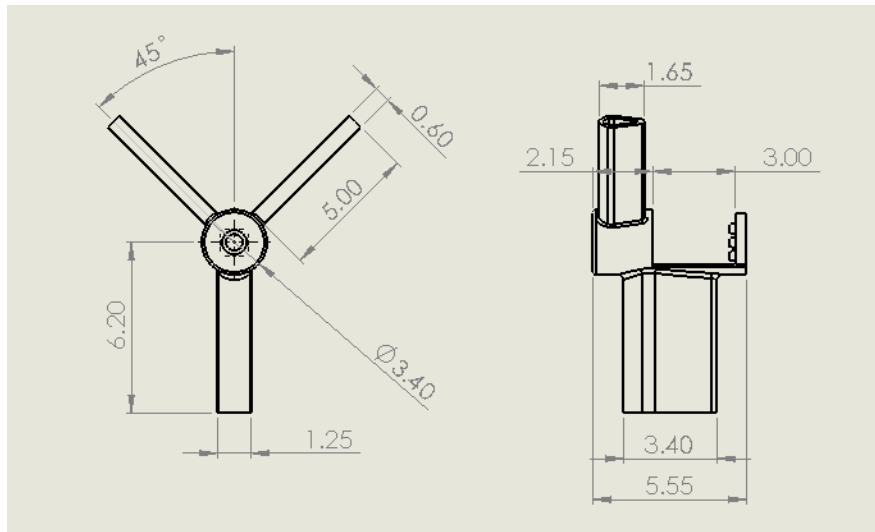
Figure 23. Nacelle drawing; units in inches.
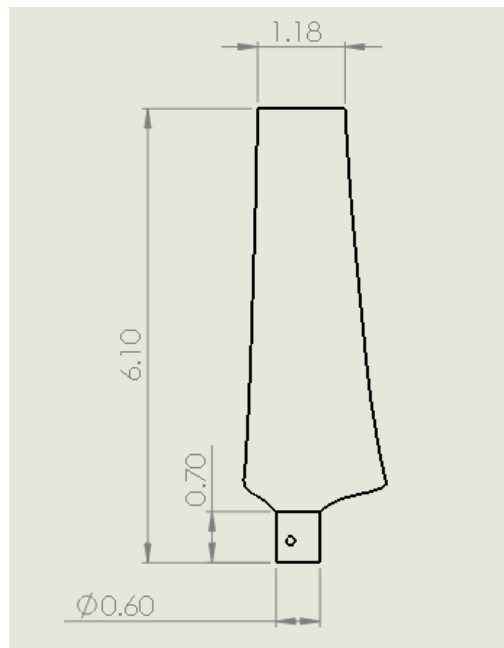
Figure 24. Blade drawing; units in inches.
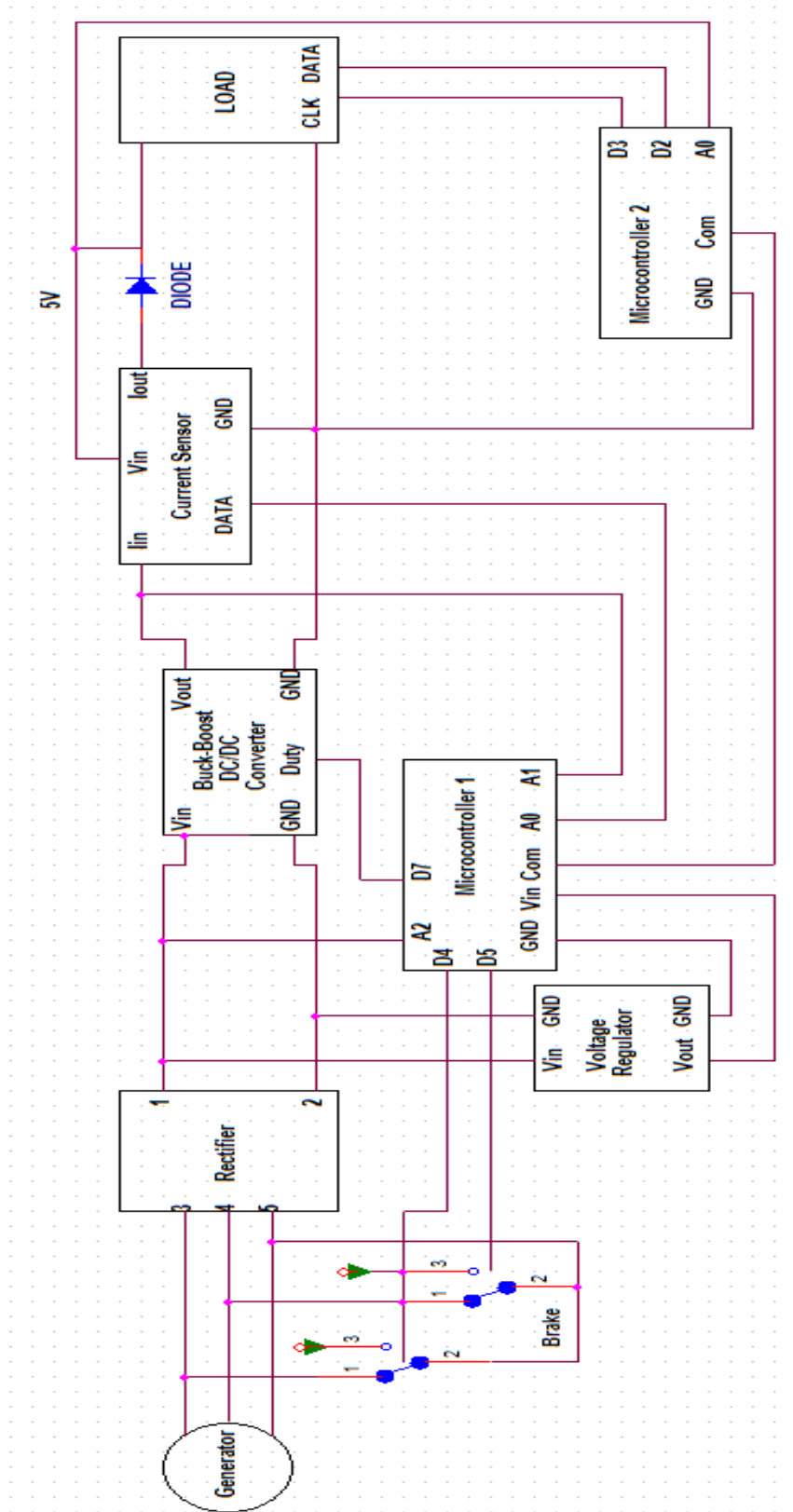
Figure 25. Reproduction of Figure 11, enlarged for clarity.

References

[1] Flannery, K., Holligan, M., & Soares, J. (2014). Shrouded small wind turbines.

[2] Yuji Ohya ve Takashi Karasudani. (2010, 30 Şubat). A Shrouded Wind Turbine Generating High Output Power with Wind-lens Technology. Molecular Diversity Preservation International.

[3] www.solidworks.com

[4] Cui, W., Liu, X., Yu, F., & Whitty, J. (2009, September). Analysis of the passive yaw mechanism of small horizontal-axis wind turbines. In World Non-Grid-Connected Wind Power and Energy Conference, 2009. WNWEC 2009 (pp. 1-5). IEEE.

[6] Tangler, J. L., & Somers, D. M. (1995). NREL Airfoil Families for HAWTs. doi:10.2172/10106095

[5] www.q-blade.org

[7] www.ni.com/labview/